

UNCLASSIFIED

|  |
|--|
|  |
|  |
|  |
| AD NUMBER  |
| ADB024098  |
| NEW LIMITATION CHANGE  |
| TO<br>Approved for public release, distribution unlimited  |
| FROM<br>Distribution authorized to U.S. Gov't. agencies only; Test and Evaluation; 01 DEC 1977. Other requests shall be referred to Space and Missile Systems Organization, Los Angeles AFB, CA 90009. |
| AUTHORITY  |
| SAMSO ltr dtd 26 Apr 1978  |

THIS PAGE IS UNCLASSIFIED

THIS REPORT HAS BEEN DELIMITED  
AND CLEARED FOR PUBLIC RELEASE  
UNDER DOD DIRECTIVE 5200.20 AND  
NO RESTRICTIONS ARE IMPOSED UPON  
ITS USE AND DISCLOSURE.

DISTRIBUTION STATEMENT A

APPROVED FOR PUBLIC RELEASE;  
DISTRIBUTION UNLIMITED.

98  
②

ADB024098

# A Phenomenological Framework for Reentry Dispersion Source Modeling

Prepared by R. H. PALMER  
Reentry Systems Division  
The Aerospace Corporation  
and  
J. J. PETTUS and R. A. LARMOUR  
General Electric Company

1 December 1977

Interim Report

Prepared for  
SPACE AND MISSILE SYSTEMS ORGANIZATION  
AIR FORCE SYSTEMS COMMAND  
Los Angeles Air Force Station  
P.O. Box 92960, Worldway Postal Center  
Los Angeles, Calif. 90009

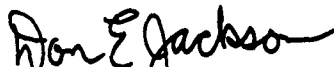
AD No. \_\_\_\_\_  
DDC FILE COPY

D D C  
RECEIVED  
JAN 13 1978  
D

DISTRIBUTION LIMITED TO U.S. GOV'T. AGENCIES ONLY;  
TEST AND EVALUATION; 1 DECEMBER 1977. OTHER REQUESTS  
FOR THIS DOCUMENT MUST BE REFERRED TO SAMSO (RSSE).

This interim report was submitted by The Aerospace Corporation, El Segundo, CA 90245, under Contract F04701-76-C-0077 with the Space and Missile Systems Organization, Deputy for Reentry Systems, P. O. Box 92960, Worldway Postal Center, Los Angeles, CA 90009. It was reviewed and approved for The Aerospace Corporation by J. F. Mullen, Reentry Systems Division. The project officer was Capt. Don E. Jackson, SAMSO (RSSE).

This technical report has been reviewed and is approved for publication. Publication of this report does not constitute Air Force approval of the report's findings or conclusions. It is published only for the exchange and stimulation of ideas.



Don E. Jackson, Capt, USAF  
Chief, Design Technology Branch  
Deputy for Reentry Systems



James M. McCormack, Lt. Col, USAF  
Chief, Reentry Technology Division  
Deputy for Reentry Systems

FOR THE COMMANDER



William Goldberg, Lt Col, USAF  
Director, Systems Technology  
Deputy for Reentry Systems



UNCLASSIFIED

SECURITY CLASSIFICATION OF THIS PAGE(When Data Entered)

19. KEY WORDS (Continued)

Ablation  
Shape Change  
Roll Torque  
Roll Resonance

20. ABSTRACT (Continued)

result, the need exists for an overall modeling framework which is both complete and flexible enough to accommodate the various phenomenological models that evolve for the contributors. This framework has been developed and is embodied in a unique hybrid computer code. The code is modular in construction enabling interchanging and upgrading of the various elements. It has proven to be a powerful tool for evaluating the BRV dispersion phenomena and for determining model and parameter sensitivities. It is constructed to allow Monte Carlo statistical studies to be conducted economically. This report provides an overview of the various dispersion-producing events and describes the code structure, modeling and application.

|                                 |  |
|---------------------------------|--|
| ACCESSION 175                   |  |
| RTIS                            | White Section <input type="checkbox"/>           |
| DDG                             | Self Section <input checked="" type="checkbox"/> |
| UNANNOUNCED                     | <input type="checkbox"/>                         |
| JUSTIFICATION.....              |  |
| BY .....                        |  |
| DISTRIBUTION/AVAILABILITY CODES |  |
| DISC.                           | STATE, GROUP & SPECIAL                           |
| B                               |  |

DDC  
RECEIVED  
JAN 13 1978  
RECEIVED  
D

UNCLASSIFIED

SECURITY CLASSIFICATION OF THIS PAGE(When Data Entered)

## CONTENTS

|     |   |    |
|-----|---|----|
| 1.  | INTRODUCTION . . . . .  | 5  |
| 2.  | LIFT-PRODUCING EVENTS . . . . .   | 11 |
| 2.1 | Initial Precessional Motion . . . . .   | 11 |
| 2.2 | First Roll Resonance . . . . .  | 11 |
| 2.3 | Boundary Layer Transition . . . . .   | 11 |
| 2.4 | Roll-Trim Variability With Roll Rates<br>Bounded Between Zero and Resonance . . . . . | 12 |
| 2.5 | Roll Trim With Roll Rate Going Through<br>Zero . . . . .                              | 12 |
| 2.6 | Roll Trim With Roll Rate Increasing to<br>or Through Resonance . . . . .              | 12 |
| 3.  | INITIAL PRECESSIONAL MOTION . . . . .   | 15 |
| 4.  | FIRST ROLL RESONANCE . . . . .  | 19 |
| 5.  | BOUNDARY LAYER TRANSITION . . . . .   | 21 |
| 6.  | NOSETIP SHAPING AND ROLL TORQUE . . . . .   | 33 |
| 6.1 | Nosetip Shape Change Effects . . . . .  | 33 |
| 6.2 | Roll Torque Effects . . . . .   | 36 |
| 6.3 | Roll-Trim Applications . . . . .  | 36 |
| 6.4 | Zero Roll Torque . . . . .  | 39 |
| 6.5 | Roll Through Zero . . . . .   | 39 |
| 6.6 | Low-Altitude Resonance . . . . .  | 41 |
| 7.  | STATISTICAL APPLICATION AND SUMMARY . . . . .   | 43 |
| 8.  | CONCLUSION . . . . .  | 45 |
|     | NOMENCLATURE . . . . .  | 47 |

## TABLES

|    |   |    |
|----|---|----|
| 1. | Dispersion Factors During Reentry . . . . .                   | 8  |
| 2. | Typical Lift-Induced Impact Point Miss Contributors . . . . . | 12 |
| 3. | Transition Sensitivity Runs . . . . .                         | 27 |
| 4. | In-Plane Transition Front Skewness Models . . . . .           | 28 |
| 5. | Body-Fixed Moment Models . . . . .                            | 28 |

## FIGURES

|     |  |    |
|-----|--|----|
| 1.  | Typical BRV Flight Profile . . . . .   | 6  |
| 2.  | Ballistic Dispersion Code Format . . . . .   | 9  |
| 3.  | Initial Precessional Motion Effects on Dispersion . . . . .                          | 16 |
| 4.  | First Roll Resonance Effects on Dispersion . . . . .                                 | 20 |
| 5.  | Idealized Transition Front Model for Aerodynamic Coefficients . . . . .              | 22 |
| 6.  | Incremental Moment and Force Coefficients Due to Transition Front Movement . . . . . | 24 |
| 7.  | Body-Fixed Moment Sensitivity Functions for $r_n/r_B = 0.1$ . . . . .                | 25 |
| 8.  | Effect of Body-Fixed Moment on Transition Motion . . . . .                           | 29 |
| 9.  | Effect of Wind Fixed Trim on Transition Motion . . . . .                             | 30 |
| 10. | Nose Recession Profiles . . . . .  | 35 |
| 11. | Trim Angle of Attack Profile . . . . .   | 35 |

PRECEDING PAGE BLANK-NOT FILMED

FIGURES (Continued)

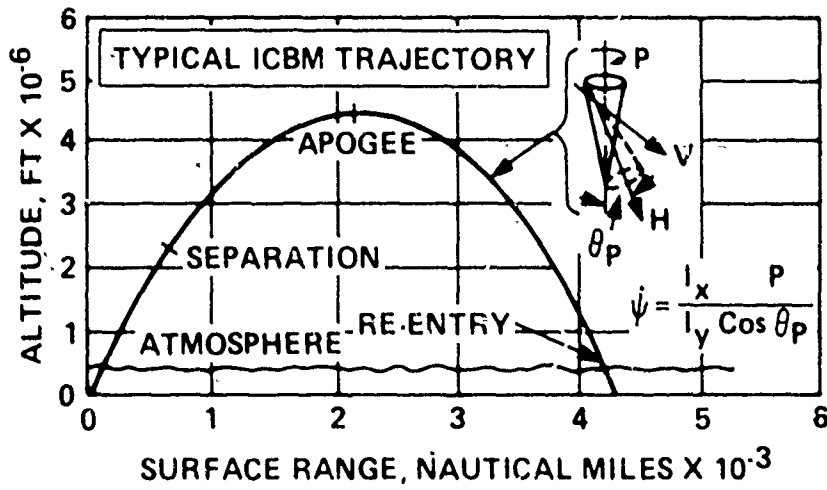
|     |  |    |
|-----|--|----|
| 12. | Typical Frustum Roll Torque Coefficient History for Ablated Shape . . . . .        | 37 |
| 13. | Roll Rate Profiles for Roll-Trim Examples . . . . .                                | 38 |
| 14. | Trajectory Deflection Angles for Spin Through Zero . . . . .                       | 40 |
| 15. | Angle of Attack at Second Resonance . . . . .                                      | 42 |
| 16. | Miss Distance Normalized to CEP Versus Cumulative Probability in Percent . . . . . | 44 |

## 1. INTRODUCTION

The delivery of a ballistic reentry vehicle (BRV) from its launch site to a target has three distinct segments. These regimes are illustrated in Figure 1 and include the boost, exoatmospheric and endoatmospheric phases. The boost phase, during which the BRV is accelerated to suborbital velocities by two or more booster stages, typically lasts only several minutes. At the end of boost, the BRV is reoriented and spin stabilized to provide an inertial attitude that is designed to produce a small angle of attack at reentry. In general, perturbations during the separation and spin-up result in the body longitudinal axis,  $X_B$ , describing a cone about the angular momentum vector, (H) which is imparted to the BRV by the spin system. The exoatmospheric portion of flight lasts for one-half hour or more for an ICBM trajectory, during which the precessional motion established at deployment is maintained unchanged. The endoatmospheric (reentry) phase is initiated when the atmosphere starts to alter this vacuum motion. This terminal phase lasts approximately a half minute.

From the standpoint of accuracy evaluation, those errors which accrue during boost and deployment, and which cause the entry state vector to deviate from that which was planned, can be divorced from those errors which develop during reentry. This report deals with the modeling and evaluation of those effects which cause the vehicle to depart from its planned flight path during the final, brief endoatmospheric flight phase.

In modeling the reentry trajectory disturbances of a BRV, it has generally been necessary to treat the dispersion mechanisms on an empirical basis rather than from first principles of aerothermodynamics. The reason for this is that uncertainties in the form and substance of the underlying phenomena are large. As a result, estimates have to be made on the basis of particular ground and flight tests scaled to the particular case under study. The motivation is strong to improve prediction capability by



$$\dot{\psi} \approx \Delta\omega + (\omega_0^2 + \Delta\omega^2)^{1/2}$$

$$\Delta\omega = \frac{I_x}{2I_y} P$$

$$\omega_0 = \sqrt{\frac{q \cdot A d C_{m\alpha}}{I_y}}$$

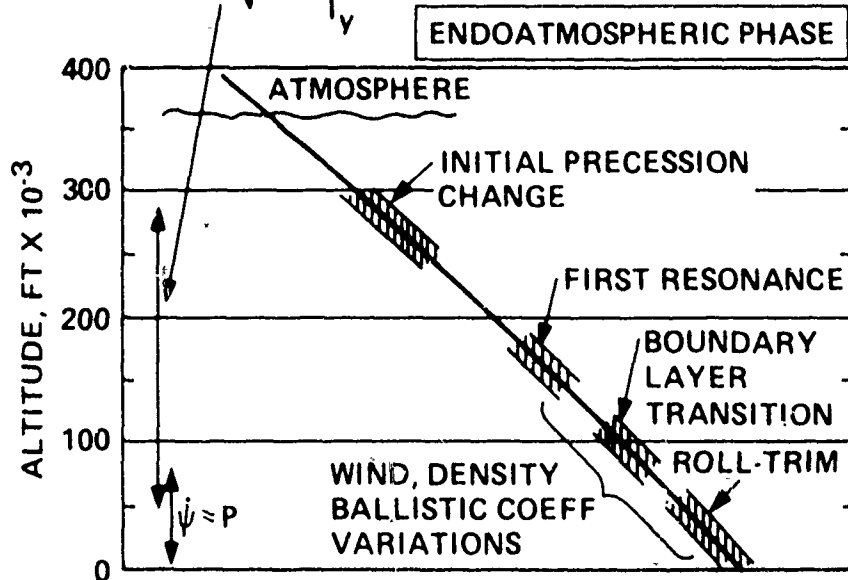


Figure 1. Typical BRV Flight Profile

replacing these empirical approximations by fundamental models. The reentry dispersion of BRV results from two categories of contributors: those perturbing the nominal drag and thus acting on the magnitude of the velocity vector; and those perturbing the lift, and thus affecting the direction of the velocity vector. Drag variations affect the trajectory curvature and thereby cause errors in range. During entry, the lift vector precesses about the velocity vector such that variations in lift produce errors which are random in direction. A summary of the factors involved in each dispersion category is given in Table 1. (Atmospheric wind is included as a lift source since it produces a change in the flight direction.) The other lift-induced errors result from variations in the lift vector magnitude and precession rate. These errors are achieved due to the development of a net incremental velocity normal to the nominal flight path caused by deviations in the lift magnitude or precession periodicity. Factors which cause these variations may result from minor protuberances or asymmetries on the vehicle surface, vehicle mass asymmetries and flow asymmetries associated with boundary layer transition.

The objective of this report is to describe a framework for inclusion of the aerothermodynamic modeling of the lift-induced trajectory errors resulting from these body and flow asymmetries. The framework is contained within the Ballistic Dispersion Code (BDC), which is a hybrid (digital and analog) six-degree-of-freedom computer program. Implicit in the code, also, are those drag-induced errors experienced due to shape change variations and vehicle dynamic response effects.

The BDC is modularized to provide the flexibility to accommodate a varied assortment of models of the error contributors. It is structured to be used in a Monte Carlo mode whenever population statistics are of interest. The code has incorporated into it a series of subroutines which internally yield the values of the prime dispersion contributors (drag changes, trim growth, meridian changes, roll torques, forces and moments at transition, etc.) given a set of critical parameters and/or mechanisms. A flow

Table 1. Dispersion Factors During Reentry

|                | Drag   | Lift   |
|----------------|--|--|
| Atmosphere     | Air Density<br>Weather (Hydrometeor Profile) | Wind Velocity and Direction  |
| Vehicle Motion | Entry Angle of Attack/<br>Convergence        | Entry Angle of Attack/Precession   |
| Vehicle        | Weight and Area Loss<br>Nose Shape Change    | Initial Mass and Configuration<br>Asymmetries<br><br>Ablation Induced Asymmetries<br>- Mass<br>- Nose Shape<br>- Shield Patterns |
| Flow Condition | Boundary Layer Transition Progression        | Boundary Layer Transition Asymmetries  |

diagram that illustrates the interactions between the basic 6DOF trajectory program and the subroutines for calculating the basic and perturbed aerodynamics is shown in Figure 2. The figure also indicates the method for operating the simulation in a Monte Carlo mode which allows for the statistical evaluation of lift effects.

The operation of the code as presented in Figure 2 is as follows. Given a basic set of vehicle parameters such as bluntness, cone angle, size, etc., basic unablated aerodynamics are determined. Using these data and the specific mass properties, the trajectory computations are initiated. At frustum transition, the baseline aerodynamics are altered in accordance with the transition aerodynamic perturbation model. The key parameters to this model are to be selected on a random sample basis. Throughout each

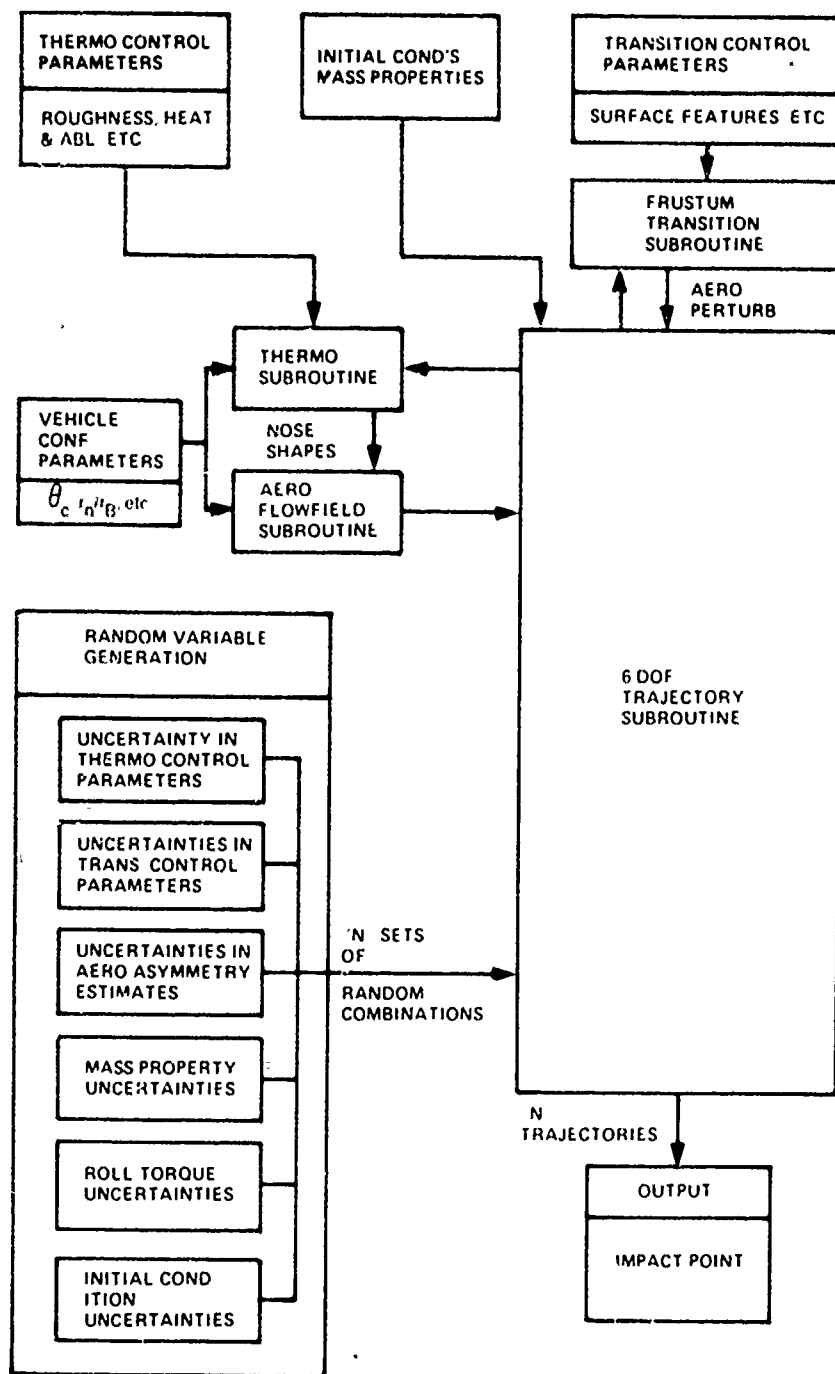


Figure 2. Ballistic Dispersion Code Format

individual simulation, thermal nose recession and shape computations are made using the developed routines. These recessions and shape computations reflect the as-computed trajectory and angle of attack. The random selections of key parameters on two rays permit the development of differing ablation and, therefore, asymmetry development. Parameters that are used in this random selection process are enumerated in Figure 2. Having developed, at a given point in the trajectory, shape and asymmetry parameters in the thermodynamic subroutine, these outputs are continuously input into the aerodynamic subroutine where changes to the vehicle drag and stability as well as trim moment and roll torque are computed. These modified aerodynamics are then used in the next trajectory computation step.

The thermodynamic and aerodynamic relationships have been segmented for simplicity in developing program modifications as state-of-the-art advancements warrant changes in the computational procedures. Furthermore, the code has been structured for future inclusion of weather erosion effects.

The hybrid computer operation of the code allows Monte Carlo studies to be conducted on an economical basis. However, because it models the thermodynamic and aerodynamic processes in some detail, the code has proven most appropriate from a total run time standpoint, to limit Monte Carlo samples to 100 trajectories. This is considered sufficient to define the population distribution in detail up to the 90th percentile. For the definition of the accumulative miss distance profile at higher probability levels, less detailed empirical modeling approaches may be used.

In the discussion that follows, the important (or potentially significant) sources of lift-induced errors are described along with the current approach to their modeling within the BDC. We start at the early reentry effects, where ablation has yet to be significant, and work down the trajectory in discussing the respective lift-producing situations modeled in the BDC.

## 2. LIFT-PRODUCING EVENTS

The sequence of lift-producing events that may be encountered as the vehicle descends through the atmosphere is given in Table 2. Representative orders of magnitude of impact point displacement are shown. The events are summarized as follows.

### 2.1 INITIAL PRECESSIONAL MOTION

At an altitude upwards of 200 kft, the established vehicle gyroscopic precessional motion is altered due to the gradually increasing aerodynamic pitch and yaw moments. The changing precessional motion can result in a brief interval during which the lift force is not averaged out. The effect on dispersion depends on the magnitude of the total angle of attack and the orientation of the precession cone at reentry.

### 2.2 FIRST ROLL RESONANCE

Between 200 and 100 kft, the aerodynamic restoring moments increase to the level where the natural pitch oscillation frequency is equal (temporarily) to the roll rate. The result is a transient divergence in angle of attack as the pitching frequency passes through the roll rate. Due to the continuous nature of the precessional motion, small impact error results provided the mass and aerodynamic asymmetries are not large.

### 2.3 BOUNDARY LAYER TRANSITION

In the general region of 100 to 50 kft, the increasing Reynolds number causes the boundary layer to begin transition from laminar to turbulent. Due to angle of attack, ablative mass transfer and surface roughness variability about the body, the transitional boundary moves non-axisymmetrically over the vehicle. Changes in the aerodynamic forces and moments accompanying the transitional process can result in the development of net lateral velocity increments which produce significant impact point displacements.

Table 2. Typical Lift-Induced Impact Point Miss Contributors

| Error Source                              | Relative Displacement Magnitude |
|---|---------------------------------|
| Initial precession                        | Small                           |
| First resonance                           | Small                           |
| Transition                                | Moderate                        |
| Roll-trim ( $0 < P < P_{CR}$ )            | Moderate                        |
| Roll through zero ( $P \rightarrow 0$ )   | Large                           |
| Roll resonance ( $P \rightarrow P_{CR}$ ) | Moderate                        |

2.4 ROLL-TRIM VARIABILITY WITH ROLL RATES BOUNDED BETWEEN ZERO AND RESONANCE

From approximately 50 kft to the impact surface, the continuing buildup in heating, aerodynamic shear and pressure cause ablation asymmetries to develop on the nose and body changing the vehicle's equilibrium roll, pitch and yaw conditions as the asymmetries change. The roll acceleration is governed by the aerodynamic roll torques which develop in flight. Varying roll rate and/or angle of attack will result in a contribution to impact miss.

2.5 ROLL TRIM WITH ROLL RATE GOING THROUGH ZERO

If the roll rate approaches or passes through zero, a vehicle with even a slight trim angle of attack may be significantly deflected from its ballistic path.

2.6 ROLL TRIM WITH ROLL RATE INCREASING TO OR THROUGH RESONANCE

If the roll rate increases to the point where it equals the natural pitch oscillation frequency, amplification of the trim angle of attack will occur, resulting in high lateral loads and induced drag. For certain

combinations of trim and c. g. offset, the roll rate will stabilize in resonance, prolonging the effects. The impact displacement is almost entirely of a range shortening type because integrated specific lift remains small due to the high uniform precessional rate of the vehicle lift vector.

Each of the above lift-producing events is modeled within a framework referred to as the Ballistic Dispersion Code. Complete trajectory calculations (either singly or in ensembles) can be made with all of the events occurring in sequence. The accommodations made in the BDC for their detailed modeling is discussed for each in turn.

### 3. INITIAL PRECESSIONAL MOTION

A spinning vehicle's precessional characteristics and angle of attack behavior during early reentry are highly dependent on the exoatmospheric coning motion and orientation. When the vehicle enters the atmosphere the aerodynamic moment acts to align it with the flight path. The gyroscopic moment developed as a result of this overturning aerodynamic moment produces varied perturbations to the precession rate and may cause a reversal in the precession direction. Platus<sup>1</sup> has shown that if the vehicle is initially coning with the flight path inside the cone, the induced gyroscopic moments will cause the precession rate to increase positively (i. e. , in the direction of the roll rate). If the initial coning motion does not circumscribe the flight path the gyroscopic action will cause the vehicle to precess negatively. Such alterations may result in net aerodynamic loading normal to the flight path and, consequently, a deflection of the trajectory.

Examples of the respective dynamics and impact point displacement computed within the BDC framework for the two types of initial coning conditions are shown in Figure 3. Type I coning is defined as not circumscribing the flight path. Type II coning does. Both sets of calculations assume a coning half-angle of 8 degrees, but the Type I run is initiated at an angle of attack maximum of 20 degrees, whereas the Type II is started at 8 degrees. For the Type II run, the precessional direction remains positive and the motion is well distributed about the flight path, resulting in no significant impact displacement. On the contrary, the Type I run demonstrates that the precession reverses and the motion is not well distributed, resulting in a moderately large impact displacement. The importance of

<sup>1</sup>D. H. Platus, "Angle-of-Attack Convergence and Windward - Meridian Rotation Rate of Rolling Reentry Vehicles," AIAA Paper No. 69-100, AIAA 7th Aerospace Sciences Meeting, New York, N. Y. , January 20-22, 1969.

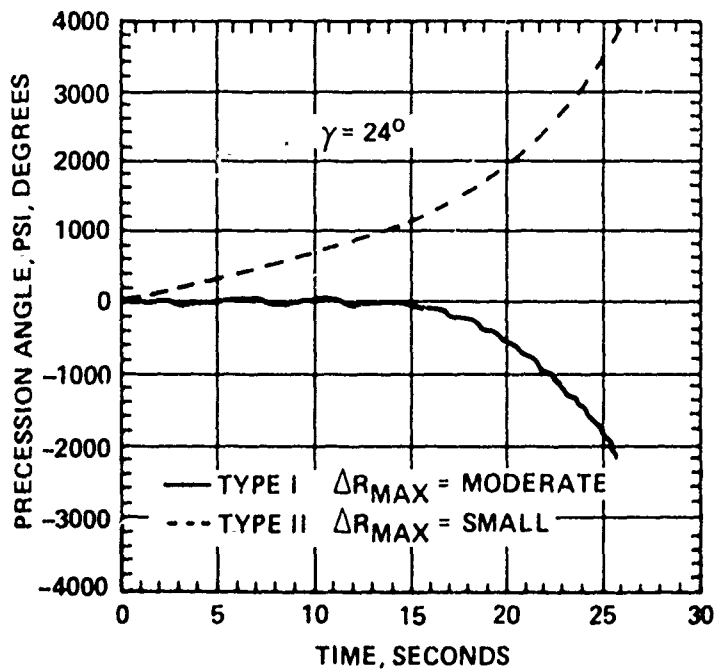
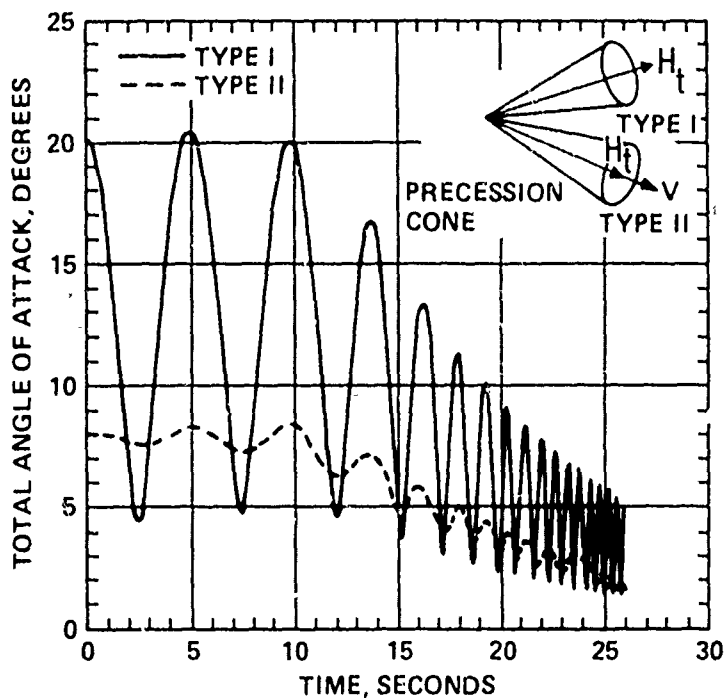


Figure 3. Initial Precessional Motion Effects On Dispersion

accurate R/V attitude control at the time of separation from the booster is well known. Estimation of initial attitude and attitude rate statistics are required in order that this particular dispersion contributor can be statistically evaluated.

#### 4. FIRST ROLL RESONANCE

The transient divergence in angle of attack due to passage of the pitching frequency through the roll rate has been well described by Kanno<sup>2</sup> and Hodapp<sup>3</sup>. The amplitude of the divergence is directly influenced by the magnitudes and combinations of the mass and aerodynamic asymmetries, and by the atmospheric density (i. e., the altitude of resonance crossing). For a particular configuration the divergence is reduced with decreasing density and steeper flight paths. An example of the application of the BDC for the evaluation of first resonance effects is shown in Figure 4. The altitude of resonance crossing is approximately 150 kft. The vehicle is assumed to have a small principal axis misalignment and a small aerodynamic trim angle in the same plane. There is also a small c. g. offset along the positive normal to this plane. This combination of configurational asymmetries produced a total angle of attack divergence of 5 degrees. Examination of the precessional parameters shows that the motion is well behaved in terms of its being distributed about the flight path. The only effect on impact miss contribution is that due to the drag induced by the angle of attack divergence, and results in a small decrease in range.

---

<sup>2</sup>J. S. Kanno, Spin-Induced Forced Resonance Behavior of a Ballistic Missile Reentering the Atmosphere, Lockheed Report LMSD-288139 (January, 1960).

<sup>3</sup>A. E. Hodapp, "Effects of Unsymmetrical Stability Derivative Characteristics on Reentry Vehicle Transient Angular Motion," AIAA Journal of Spacecraft and Rockets, 13, (2), 82 (February 1976).

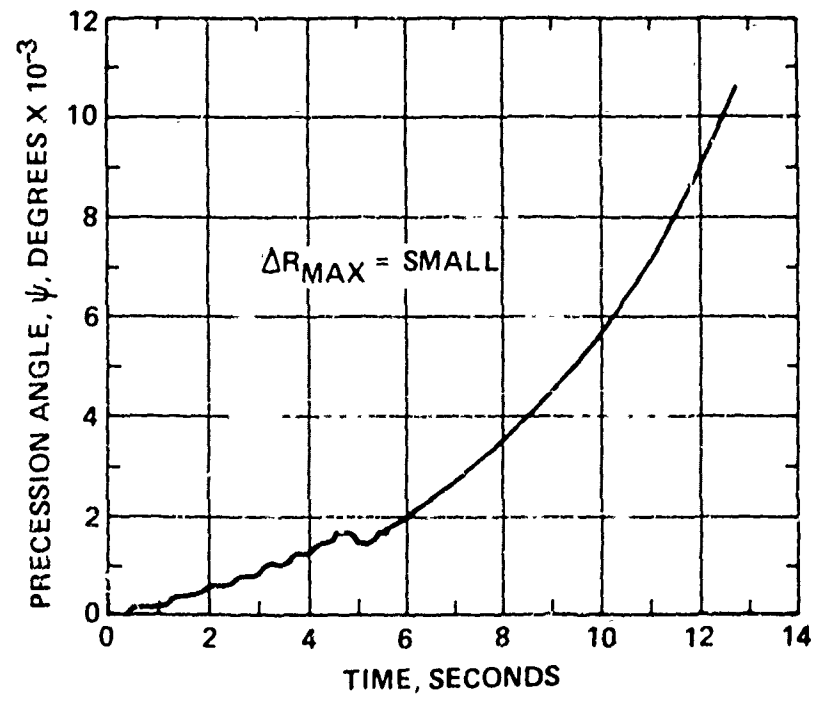
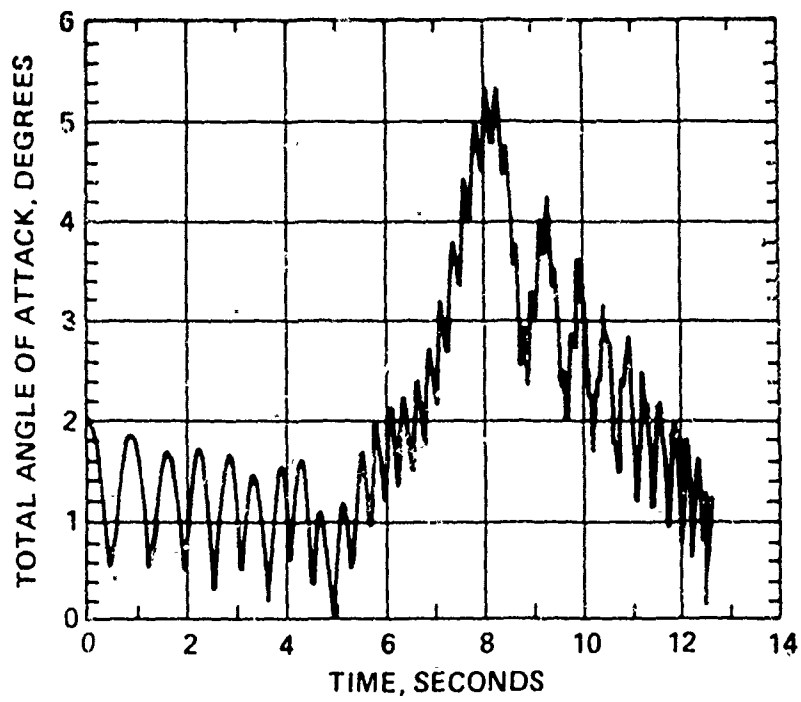


Figure 4. First Roll Resonance Effects on Dispersion

## 5. BOUNDARY LAYER TRANSITION

As the vehicle passes from the laminar boundary layer condition to fully turbulent, the aerodynamics of the vehicle are changed. The transition in the aerodynamics is irregular and dependent on the progression of transition over the body. Because boundary layer transition is coupled with angle of attack, a model which includes a representation for both is necessary. The rigid body dynamics are governed by aerodynamic forces and moments which are functions of transition status, which in turn is a function of angle of attack and other input parameters.

Vehicle dynamics during the time transition progresses over the body respond in various ways, depending on factors such as frustum mass addition rates and ablation lags, surface properties, aerodynamic static margin and the state of the motion prior to transition. Chrusciel<sup>4</sup> and Platus<sup>5,6</sup> found that forces and moments out of the angle of attack plane were instrumental in causing momentary divergences. Platus also showed that in-plane forces and moments coupled with independent out-of-plane values could, in principle, form the basis of the transitory dynamics modeling. Chrusciel showed the success of such an approach by application to test data. This general modeling approach has been adopted in the BDC framework.

The incremental transitional aerodynamics have been modeled in two parts, as shown in Figure 5. The first part accounts for the aerodynamic alteration in-plane as the transition front moves forward. The front is

---

<sup>4</sup>G. T. Chrusciel, "Analysis of Reentry Vehicle Behavior During Boundary Layer Transition," AIAA Journal, 13 (2), 154 (February 1975).

<sup>5</sup>D. H. Platus, "Angle-of-Attack Control of Spinning Missiles," AIAA Journal of Spacecraft and Rockets, 12 (4), 228 (April 1975).

<sup>6</sup>D. H. Platus, "Dispersion of Spinning Missiles Due to Lift Nonaveraging," Proceeding of the AIAA 3rd Atmospheric Flight Mechanics Conference, Arlington, Texas (June 7-9, 1976).

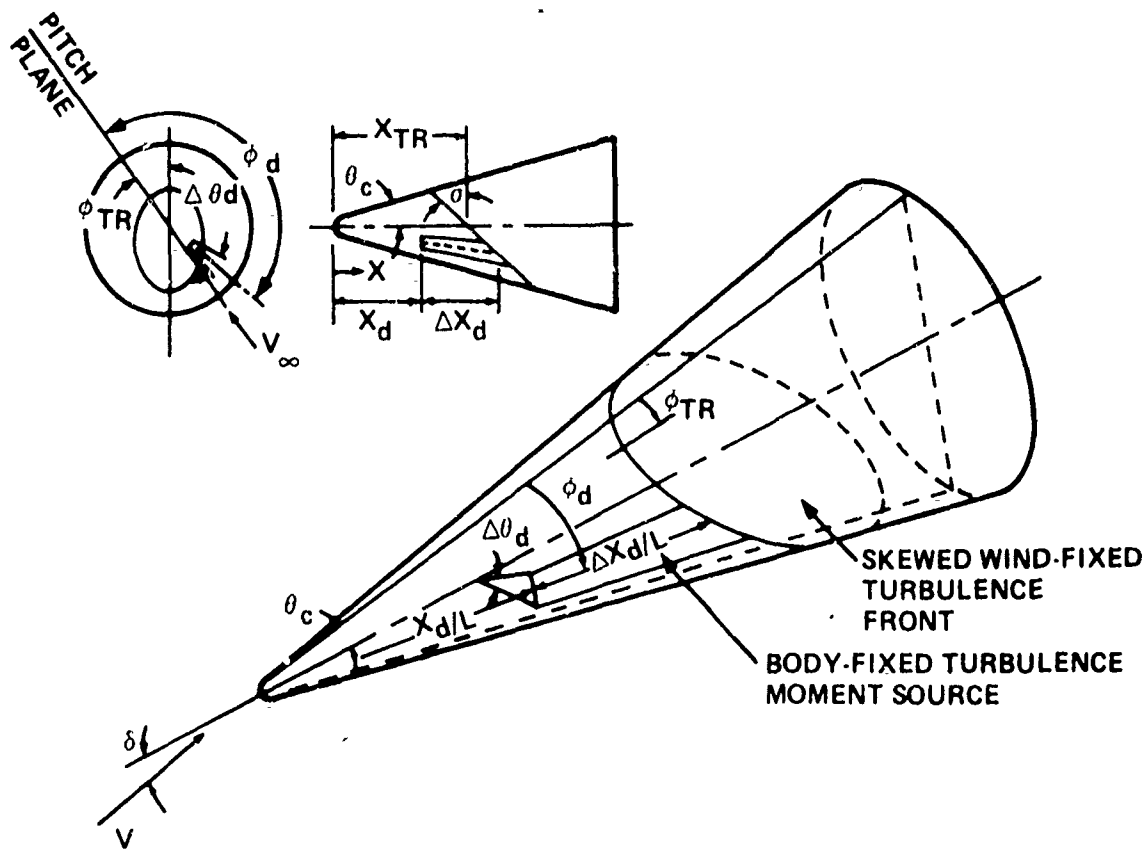


Figure 5. Idealized Transition Front Model for Aerodynamic Coefficients

assumed to lie in a plane cutting the vehicle at an angle,  $\sigma$ , to the normal to the roll axis. This angle, called the skewness angle, is defined as being a function of the instantaneous angle of attack and the mean transition front axial progress,  $X_{TR}/L$ . The model also provides for the front to be tilted out of the angle of attack plane through the angle,  $\phi_{TR}$ , which measures the angular displacement of the most forward point on the front relative to the leeward meridian (Figure 5).

The incremental aerodynamics are described as:

$$\begin{aligned}
 \Delta C_{m_{PI}} &= C_{m_T} R \cos \phi_{TR} + \Delta C_{m_\delta}^\delta \\
 \Delta C_{n_{PI}} &= C_{m_T} R \sin \phi_{TR} \\
 \Delta C_{Y_{PI}} &= C_{F_T} S \sin \phi_{TR} \\
 \Delta C_{Z_{PI}} &= C_{F_T} S \cos \phi_{TR} - \Delta C_{N_\delta}^\delta
 \end{aligned}
 \tag{1}$$

A three-dimensional-flowfield code was utilized to generate a matrix of aerodynamic data for various values of  $\sigma$ ,  $\phi_{TR}$  and  $X_{TR}/L$  and vehicle configurations. Typical incremental adjustments to the laminar aerodynamics are shown in Figure 6.

The second part of the transition model is an attempt to account for effects of body-fixed moments which may develop on a meridian  $\phi_d$ . The magnitude of body-fixed moments depends on the transition front location  $X_{TR}$ .

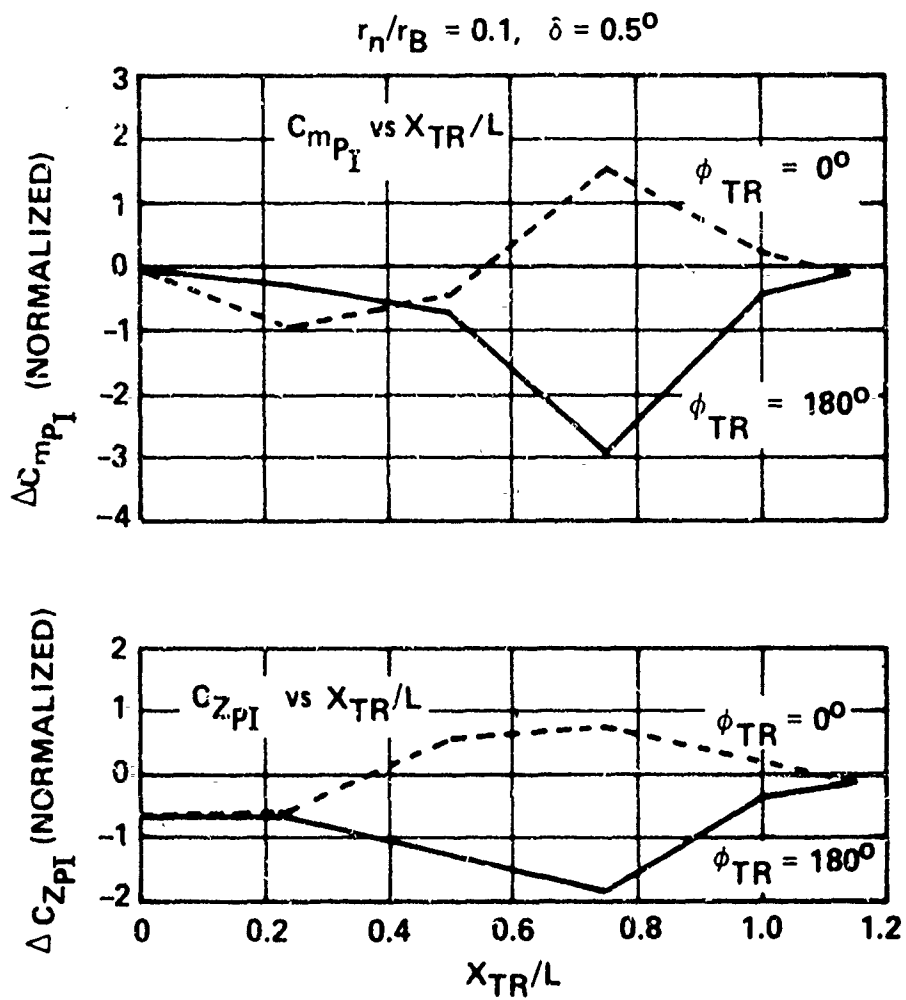


Figure 6. Incremental Moments and Force Coefficients Due to Transition Front Movement

These incremental aerodynamics are given by:

$$\begin{aligned}\Delta C_{m_{PII}} &= -G \cos \phi_d \\ \Delta C_{n_{PII}} &= G \sin \phi_d \\ \Delta C_{Y_{PII}} &= -F \sin \phi_d \\ \Delta C_{Z_{PII}} &= F \cos \phi_d\end{aligned}\tag{2}$$

where F and G are functions of the body-fixed moment parameters, and the primary front location,  $X_{TR}/L$ . Typical variations of F and G are shown in Figure 7.

Many runs were made to assess the effects of the various transition front parameters within the assumed modeling context. An investigation was made of the effects of out-of-plane tilt, body-fixed moment parameters, in-plane skewness, and initial motion conditions, in various combinations. An enumeration of the runs and principal results is made in Table 3. The details of the models used are given in Table 4 and Table 5. The results show that the dynamic perturbations and impact displacements vary widely.

For a moderately skewed front with windward side forward and without body-fixed moment parameters (Case 1, Figure 8) very little trajectory disturbance was obtained. The occurrence of relatively large body-fixed moments on the vehicle (Case 5, Figure 8) resulted in a moderate contribution to impact miss, and an angle of attack divergence to 0.7 degree and a precessional motion which temporarily reversed in direction.

A large contribution to impact miss was obtained when the transition front was allowed to be skewed to a greater extent with angle of attack using skewness model 4 (Table 4) and orienting the front leeward side forward. Such a situation (Case 24) is illustrated as the third example in Figure 9.

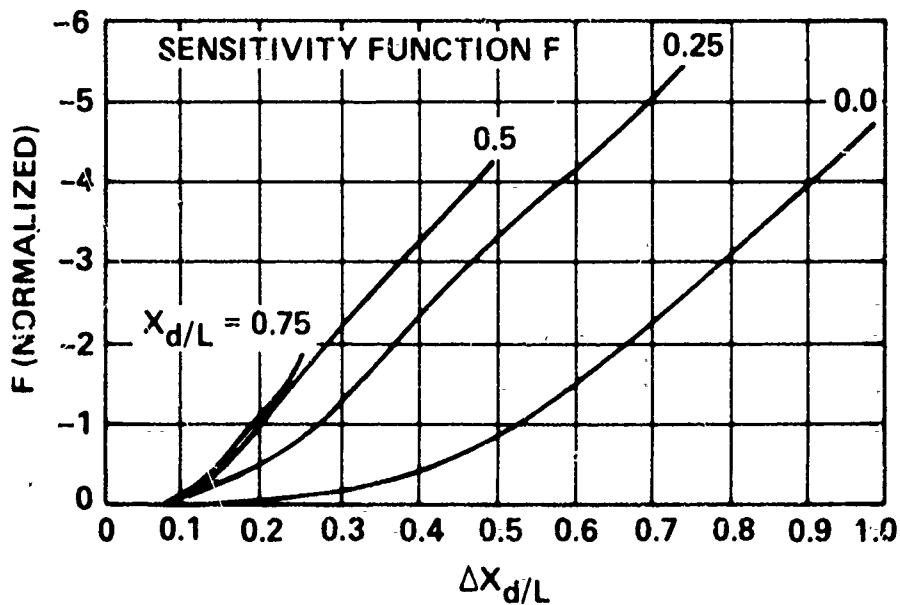
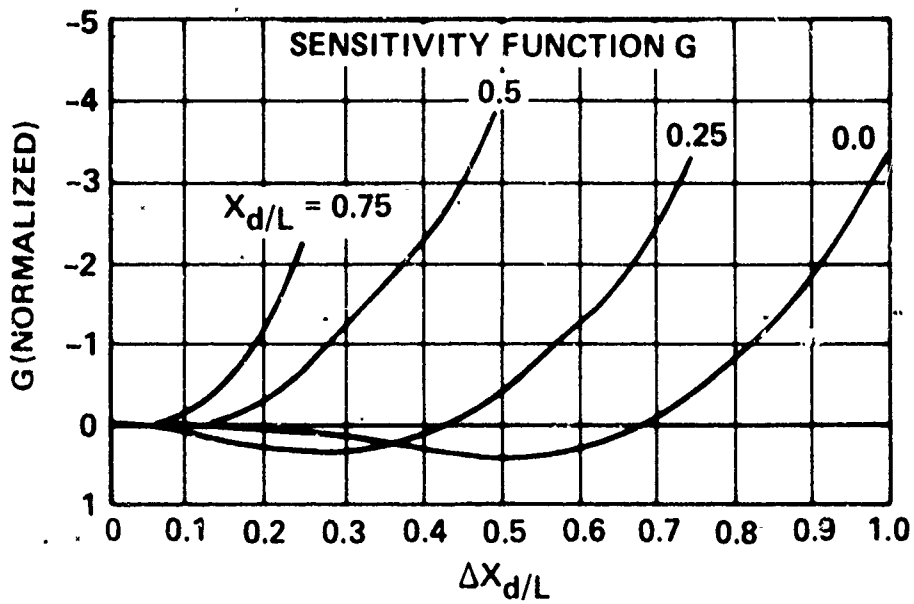


Figure 7. Body-Fixed Moment Sensitivity Functions  
for  $r_n/r_B = 0.1$

Table 3. Transition Sensitivity Runs

| Run | $\sigma/\delta$<br>Model<br>(Table 4) | $\phi_{TR}$<br>(deg) | Body-Fixed<br>Moment<br>Parameters<br>(Table 5) | Initial<br>Angle of<br>Attack (deg) | $\Delta\delta_{Max.}$<br>(deg) | Number of $\nu$<br>Reversals/<br>Changes | $\Delta R_{Max.}$<br>(ft)    | Objective   |
|-----|---------------------------------------|----------------------|---|-------------------------------------|--------------------------------|--|------------------------------|---|
| 1   | 1                                     | 180                  | 0   | 0.3                                 | ~0                             | 0  | Small                        | Front<br>Orientation<br>Effect                                  |
| 2   | 1                                     | 0                    |   |                                     | ~0                             | 0  |                              |   |
| 3   | 1                                     | 170                  |   |                                     | 0.03                           | 0  |                              |   |
| 4   | 1                                     | 135                  |   |                                     | 1.40                           | 0  |                              |   |
| 5   | 1                                     | 180                  | 1   | 0.3                                 | 0.60                           | 4  | Moderate                     | Front<br>Orientation<br>Effect<br>With<br>Body-Fixed<br>Moments |
| 6   | 1                                     | 0                    |   |                                     | 0.53                           | 2  |                              |   |
| 7   | 1                                     | 170                  |   |                                     | 0.56                           | 2  |                              |   |
| 8   | 1                                     | 10                   |   |                                     | 0.56                           | 4  |                              |   |
| 9   | 1                                     | 135                  |   |                                     | 1.32                           | 2  |                              |   |
| 10  | 1                                     | 180±10 <sup>a</sup>  |   |                                     | 0.54                           | 4  |                              |   |
| 11  | 1                                     | 180±45 <sup>a</sup>  |   |                                     | 0.83                           | 4  |                              |   |
| 12  | 1                                     | 180±90 <sup>b</sup>  |   |                                     | 0.46                           | 2  | Small                        |   |
| 13  | 1                                     | 180                  | 2   | 0.3                                 | 0.18                           | 2  | Moderate                     | Body-Fixed<br>Moment<br>Effect                                  |
| 14  | 1                                     |                      | 3   |                                     | 0.05                           | 2  | Small                        |   |
| 15  | 1                                     |                      | 4   |                                     | 0.03                           | 2  | Small                        |   |
| 16  | 1                                     |                      | 5   |                                     | 0.11                           | 2  | Moderate                     |   |
| 17  | 2                                     | 180                  | 1   | 0.3                                 | 0.44                           | 4  | Moderate                     |   |
| 18  | 2                                     | 0                    | 1   |                                     | 0.77                           | 2  |                              |   |
| 19  | 3                                     | 180                  | 1   |                                     | 0.35                           | 4  |                              |   |
| 20  | 3                                     | 0                    | 1   |                                     | 0.97                           | 2  |                              |   |
| 21  | 4                                     | 180                  | 1   |                                     | 0.11                           | 2  |                              |   |
| 22  | 4                                     | 0                    | 1   |                                     | 1.19                           | 2  |                              |   |
| 23  | 4                                     | 180                  | 0   |                                     | ~0                             | 0  | Large<br>Small<br>Very Large | Front<br>Skewness<br>Effect                                     |
| 24  | 4                                     | 0                    | 0   |                                     | 0.47                           | 2  |                              |   |
| 25  | 1                                     | 180                  | 1   | 0.15                                | 0.71                           | 3  | Moderate                     | Initial<br>Condition<br>Effect                                  |
| 26  | 1                                     |                      | 1   | ~0 <sup>c</sup>                     | 0.46                           | 4  |                              |   |
| 27  | 1                                     |                      | 1   | 2.0                                 | 0.15                           | 2  |                              |   |

<sup>a</sup> Front oscillated 8 cps  
<sup>b</sup> Front oscillated 4 cps  
<sup>c</sup> Started at null point,  $\alpha_{i,MAX.} = 0.3^\circ$

Table 4. In-Plane Transition Front Skewness Models  
( $\sigma$  vs  $\delta$ )

| Model | Linear Variation                   |                               |
|-------|------------------------------------|-------------------------------|
|       | Angle of Attack,<br>$\delta$ (deg) | Skew Angle,<br>$\sigma$ (deg) |
| 1     | 0                                  | 0                             |
|       | $\geq 1.0$                         | 45                            |
| 2     | 0                                  | 0                             |
|       | $\geq 0.5$                         | 45                            |
| 3     | 0                                  | 0                             |
|       | $\geq 0.3$                         | 45                            |
| 4     | 0                                  | 0                             |
|       | $\geq 0.1$                         | 60                            |

Table 5. Body-Fixed Moment Models

| Model | Moment Structure | $X_d/L$       | $\Delta\phi_d$ | Moment Strength |
|-------|------------------|---------------|----------------|-----------------|
| 0     | 0                | --            | --             | --              |
| 1     | Simple           | 0             | -90            | Large           |
| 2     | ↓                | 0             | -90            | Moderate        |
| 3     | ↓                | 0.35          | 90             | ↓               |
| 4     | ↓                | 0.70          | -90            | ↓               |
| 5     | Complex          | (Distributed) |                | ↓               |

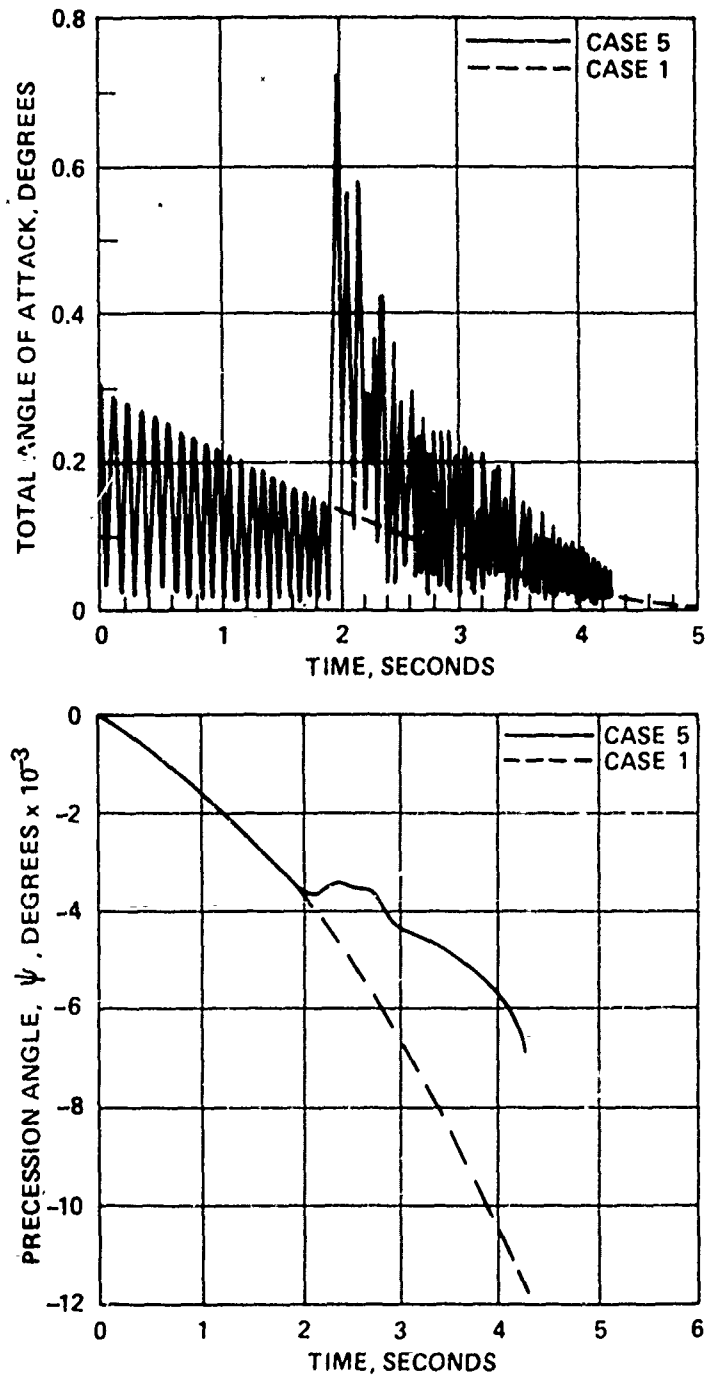


Figure 8. Effect of Body-Fixed Moment on Transition Motion (Cases 1 and 5)

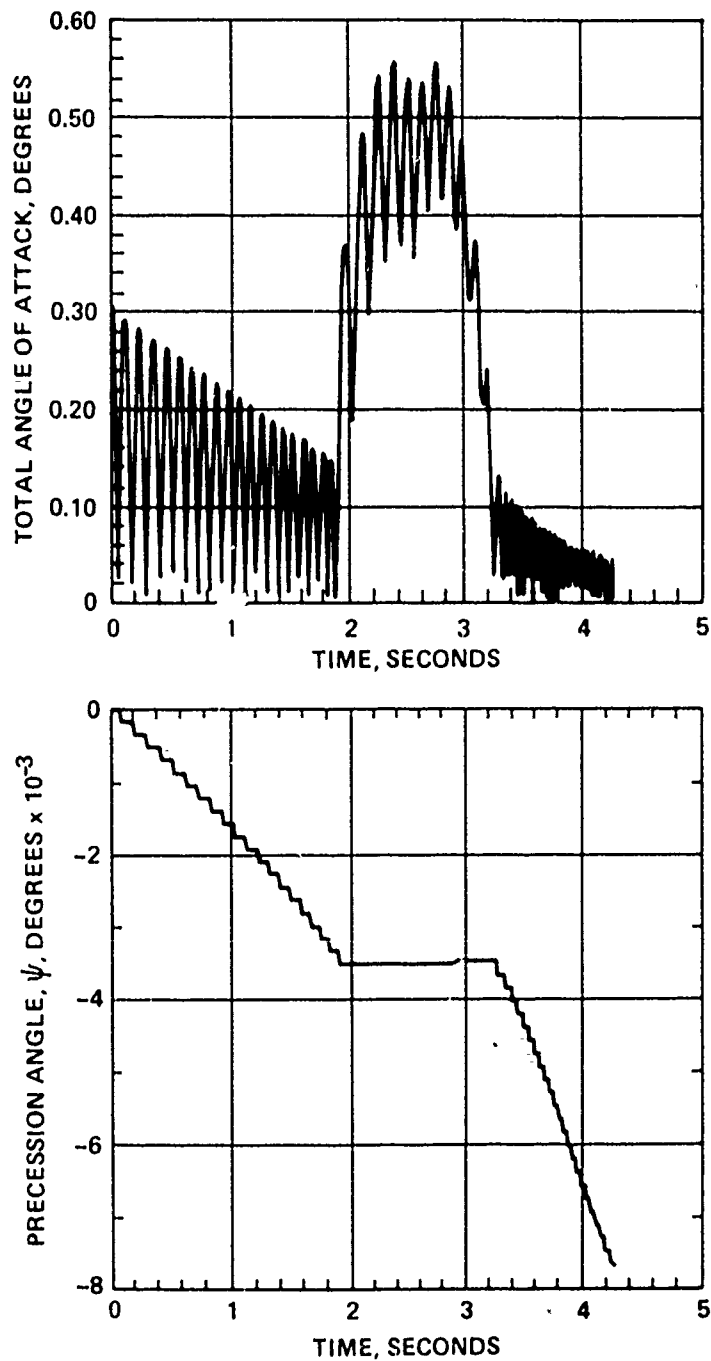


Figure 9. Effect of Wind Fixed Trim on Transition Motion

Here the effect of the highly skewed front and meridian orientation produces a situation like that described by Platus.<sup>6</sup> That is, the moment coefficient modification results in the establishment of a wind-fixed trim. This results in a condition for which the precession is nearly halted and a pronounced lateral deflection is produced. This extreme case illustrates the breadth of conditions accommodated in the framework.

Additional sensitivities were investigated by introducing deviations from the more moderate conditions defined by Case 5. The effect of varying body-fixed moment parameters showed that the miss contributors for these moderate front movement conditions varied inversely with body-fixed moment magnitude. (It is interesting to note that when a body-fixed moment was added to the extreme conditions defined by Case 24, such as in Case 22, that the miss contribution was reduced since this body-fixed disturbance did not allow the precession to be stopped as was the situation for Case 24.) The effects of tilting the transition front out of the wind plane were also examined. It was found that a fixed out-of-plane tilt could cause the angle of attack to be significantly increased. The resulting trajectory deflection was found to be moderate, however, because the motion growth was relatively smooth and the forces were integrated out (Cases 4 and 9 for instance). The effect of an oscillating front out of the wind plane was found to have similarly moderate effects (Cases 10, 11 and 12). The variation of initial conditions had only a moderate effect with the modeling considered. The disturbance and resulting dispersion were found to be reduced with initial angle of attack. Additional detailed characterization is required in order to effectively use the framework for predictions.

## 6. NOSETIP SHAPING AND ROLL TORQUE

During the late portion of flight the reentry vehicle is subjected to a severe thermal environment and heatshield ablation is accelerated. The rapid removal of material during this period generally results in the development of asymmetries in the vehicle nosetip and frustum. The aerodynamic trim and roll torque variations which result produce a class of lift-induced dispersions collectively called roll-trim errors. The vehicle nose shape development is the primary factor governing force and moment coefficient variations. To account for these effects subroutines for computing nosetip shaping and attendant aerodynamic changes are included in the BDC framework. Along with the lateral aerodynamic variations, which affect the lift-induced roll-trim performance, the nosetip shaping routine also provides drag coefficient histories for computing drag-induced effects due to ablation. A separate module is provided for computing roll torque resulting from shield ablation.

### 6.1 NOSETIP SHAPE CHANGE EFFECTS

The nosetip shaping routine accommodates both axisymmetrical and nonaxisymmetrical recession due to ablation. Two elements of the framework comprise the portion that models trim angle of attack: a nose shape model and a flowfield model. At present, the code uses a simple "in-plane" asymmetry formulation\* that will be replaced with a more general model (such as that developed by Dirling and Swain<sup>7</sup>, as a future upgrade. The flowfield<sup>8</sup> is three-dimensional, simplified from the GE-3D Flowfield

\* Unpublished Study by D. Brant.

<sup>7</sup> R. D. Dirling and C. E. Swain, "Effects of Nosetip Asymmetries on Reentry Vehicle Aerodynamics and Dispersion," Proceedings of the AIAA 4th Atmospheric Flight Mechanics Conference, Hollywood, Florida (August 8-10, 1977).

<sup>8</sup> D. W. Hall and D. T. Nowlan, "Aerodynamics of Ballistic Reentry Vehicles with Asymmetric Nosetips," AIAA Paper No. 77-701, AIAA 10th Fluid and Plasma Dynamics Conference, June 1977.

Code, and cast into a form useful for the specific objective of computing the static aerodynamics at closely spaced time intervals along the trajectory.

The stochastic behavior of the trim produced by nose asymmetry is simulated by assuming boundary layer transition on the nosetip to be initiated by a random surface roughness height. By this means, one side of the nosetip achieves transition prior to the other side, thus initiating a nonaxisymmetric recession and its associated trim angle of attack.

An example of the code's computation of a typical nose asymmetry history is shown in Figure 10. The case illustrated pertains to a slender ( $r_n/r_B = 0.1$ ) sphere-cone vehicle with an initial nose radius of 1.0 inch. Transition was induced at 34 kft on the top side but did not occur on the bottom until 27 kft, resulting in the asymmetrical shape shown. The aerodynamic coefficients for the nose shape are computed in the internal routine. It is important to note that whole-body computations are made so that downstream influences resulting from nose shaping are included in the aerodynamic computations.

The trim angle resulting from the asymmetric nose shape of Figure 10 is presented in Figure 11. The trim is initiated as the first side becomes turbulent and continues to grow until about 20 kft altitude where a peak trim of 0.34 degrees is attained. Subsequently, the trim begins to decrease somewhat as the nose tends toward more symmetry. At very low altitude, the trim again increases.

Since the current routine computes the asymmetry as if it were contained in a single plane, and since meridian changes can influence roll-trim performance, an auxiliary routine is overlaid which causes the prime trim plane to be shifted in accordance with randomly selected meridian histories. Thus the trim shown in Figure 11 is allowed to move about the body. When a more general (3D) nose shape model is incorporated this artifact may be superfluous and could be replaced by the natural meridian variations produced as the nose shape evolves.

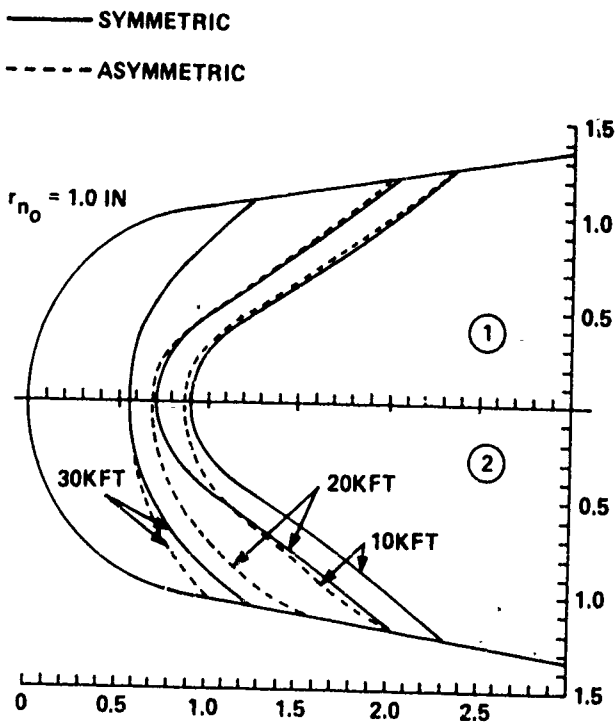


Figure 10. Nose Recession Profiles (inches)

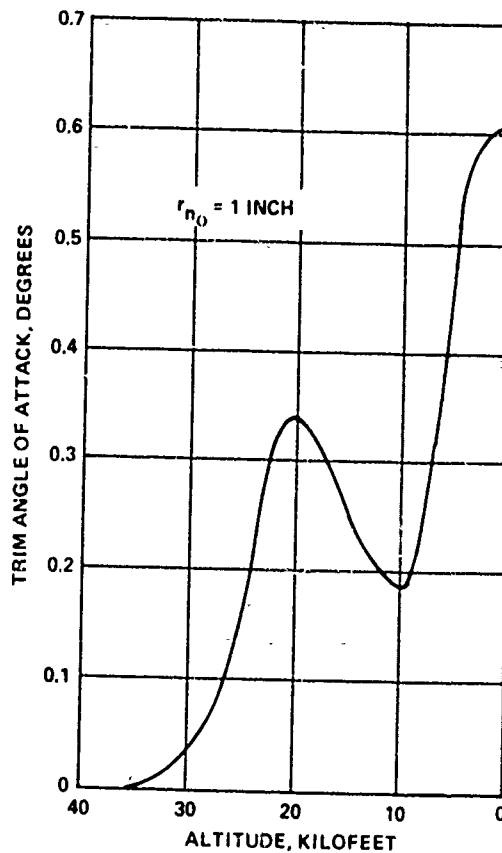


Figure 11. Trim Angle of Attack Profile

## 6.2 ROLL TORQUE EFFECTS

Typically frustum shield ablation produces surface discontinuities that result in roll torques which are initiated following frustum boundary layer transition and persist thereafter. Frustum torques for some tape wound vehicles have been shown to be correlated with the direction and number of tape laps that exist in the shield as a result of the tape winding process. Presently the Ballistic Dispersion Code utilizes an algorithm for roll torque coefficient that is based on this type of correlation. Another correlation would be required for nontape-wrapped vehicles or vehicles protected with different materials. In this model, the effect of the laps is characterized by assuming the development of a small step (forming a finlet) at each tape lap, with geometrical properties of the step tied to the tape and tape lap dimensions. The equation (Figure 12) takes into account the number, location, orientation and thickness of the finlets. The model also accounts for the boundary layer conditions that exist at finlet locations. These flow conditions and resulting roll torque are computed in a three-dimensional viscous boundary layer code.

The stochastic behavior of the frustum-produced roll torque in the BDC model is obtained in part through tolerances assumed in the finlet effectiveness. These tolerances are derived so as to accommodate variability observed in experimental data. A typical normalized roll torque variation with altitude is shown in Figure 12.

## 6.3 ROLL-TRIM APPLICATIONS

To illustrate the scope of potential roll-trim effects three cases are considered (Figure 13) representing three classes of roll-trim coupling situations. The cases examined include a nearly constant roll rate situation, a case in which a period of zero roll rate is achieved, and a case in which low altitude resonance is experienced.

$$C_{L_o} = \frac{C_D h l \cos \lambda \sin^2 \lambda \sin \nu}{2 q_\infty R_B^3 \tau_L \sin \theta_c} \int_{r_1}^{r_2} (\rho u^2)_h r^2 dr$$

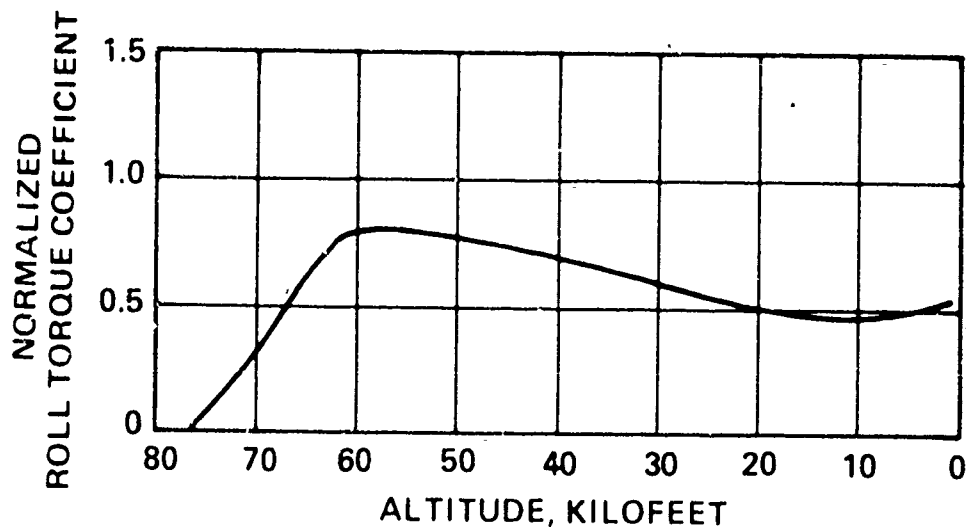


Figure 12. Typical Frustum Roll Torque Coefficient History for Ablated Shape

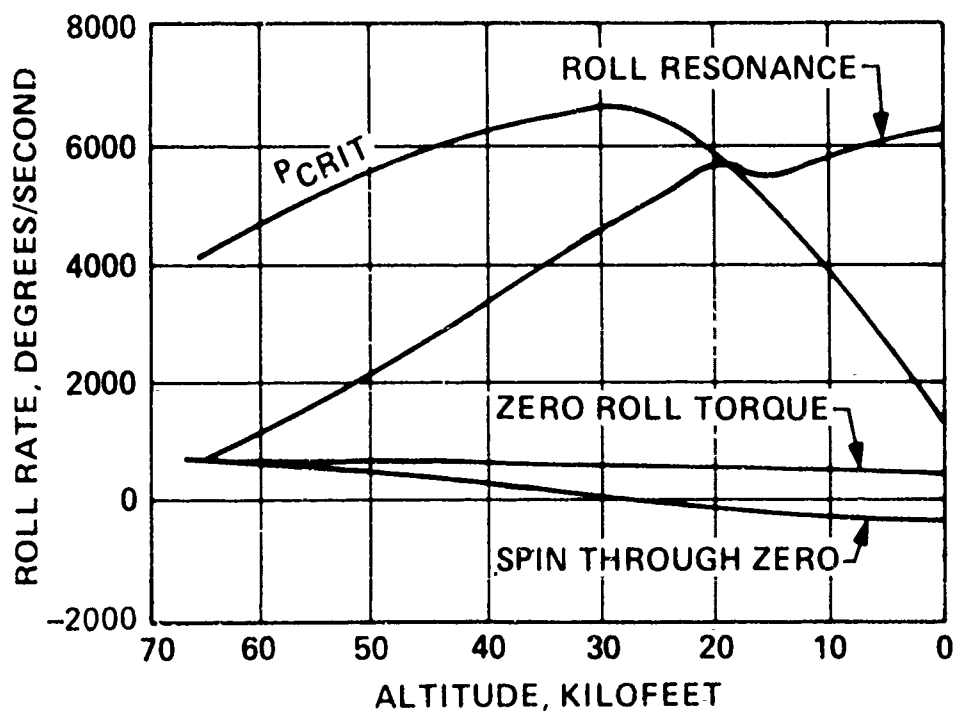


Figure 13. Roll Rate Profiles for Roll-Trim Examples

#### 6.4 ZERO ROLL TORQUE

By controlling the tape lap geometry produced in manufacturing, the frustum induced roll torque can be essentially nulled out. Computations with the previous trims, with the assumption that nose torques and c. g. effect are zero, result in motion histories that produce impact points with moderate contributions to impact miss.

#### 6.5 ROLL THROUGH ZERO

Although a level of roll rate control is passively achievable through the tape lap design, it is necessary to examine the effects of variations. For illustration, an extreme situation was simulated for which the torque was allowed to be negative in value throughout the trajectory. The resulting roll rate as illustrated in Figure 13 reaches zero at 22 kft altitude. The simulation included the same nose ablation parameters, nose geometry and trim profiles shown above. The roll through zero results in the potential for a large trajectory deflection as analytically described in Reference 9.

$$\Delta Y = \frac{C_{N_\infty} \delta_{T_S}}{m} \sqrt{\frac{-\rho_S A l_X \pi}{d C l_G}} \quad (3)$$

where the subscript S refers to the conditions at zero spin rate. For the condition shown, this results in a total trajectory deflection of nearly 3 degrees. The BDC simulation provided path angle and azimuth variation histories as shown in Figure 14 which yield a total deflection similar in magnitude to that obtained analytically. The resulting maximum impact error is very large. Thus, zero roll rate miss contribution effects are seen to be large even for moderate trim levels. Such conditions are usually

<sup>9</sup>R. A. Larmour, Analytical Method for Determining Range Error Due to Trim and Zero Roll Rate, General Electric Fundamental Memo, FM-92 (February 6, 1967).

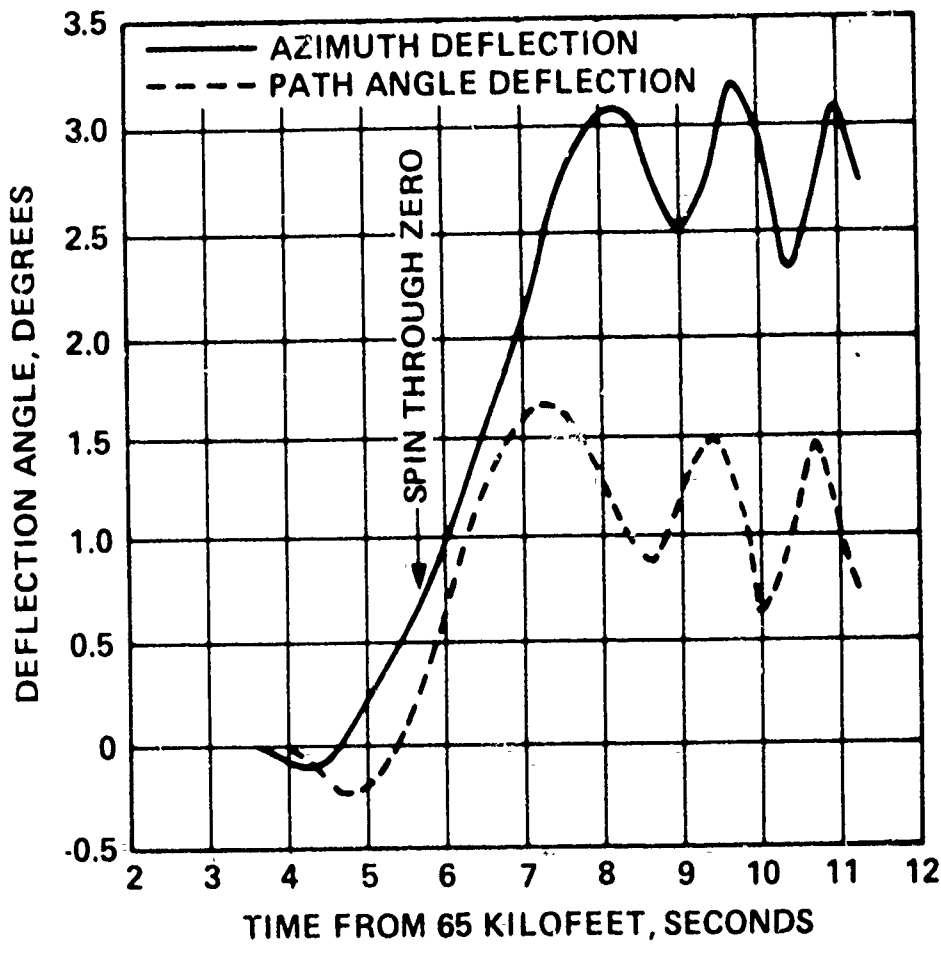


Figure 14. Trajectory Deflection Angles for Spin Through Zero

avoided in practice but are included in the framework to enable computation of sensitivities for parameter variation studies.

#### 6.6 LOW-ALTITUDE RESONANCE

The effects of low altitude resonance are included implicitly in the six-degree-of-freedom equations of motion used in BDC. To illustrate the effect of a second resonance, a roll torque history which produced a resonance encounter at 19 kft is shown in Figure 13. The resulting total angle of attack reached 4.2 degrees due to resonance amplification as shown in Figure 15. This resonance event caused only a moderate miss distance in the range shortening direction, since for this situation, resonance lock-in was not achieved. Resonance encounter is included along with the other roll-trim situations for a complete ensemble of dispersive phenomena possibilities.

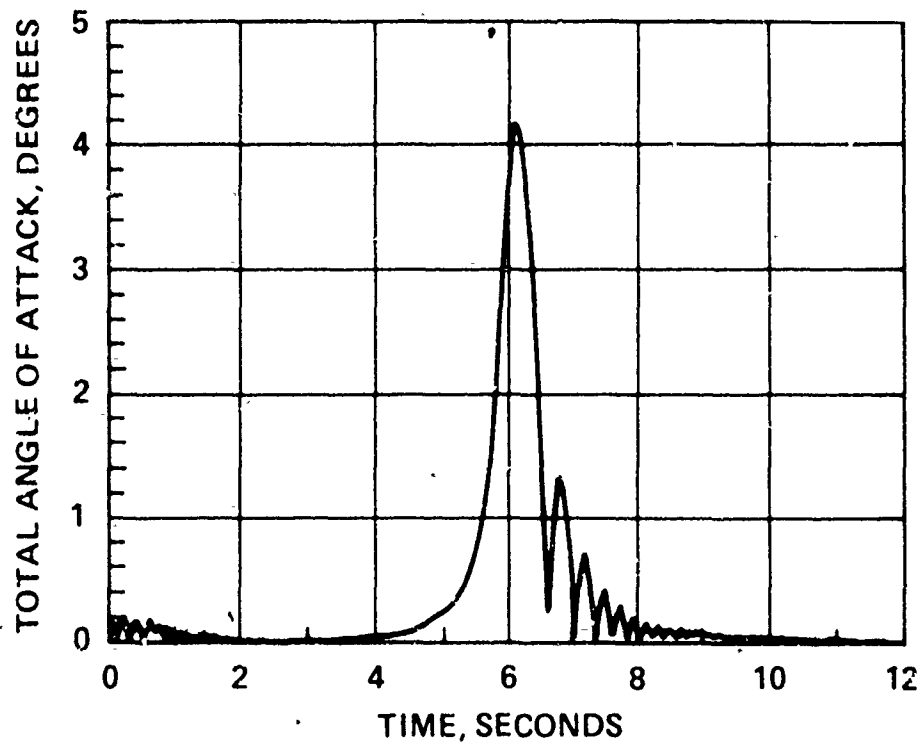


Figure 15. Angle of Attack at Second Resonance

## 7. STATISTICAL APPLICATION AND SUMMARY

The modeling described has been included in the Ballistic Dispersion Code framework for evaluating composite dispersion. The code accounts for the dynamics of each lift-induced error and provides a basis for describing the aerothermal interactions that influence them. The code has been formulated for use in a Monte Carlo fashion so that total reentry error distributions can be produced. In the formulations, statistical variations in the primary parameters provide the run-to-run variability. By reducing the sources of error to basic phenomenological mechanisms, the potential for evaluating the effects of variations in vehicle design requirements exists.

An example of a typical statistical result is shown on Figure 16. The miss distribution, normalized with CEP, indicates the non-Gaussian error population which is, in general, expected. The deviation from a Gaussian distribution may be particularly marked at the extreme cumulative probability levels because of occasional roll rate excursions near zero.

Before statistical applications of the phenomenological models can be predictively employed, it is necessary to model the definitive characteristics of the stochastic behavior of the basic phenomena. This will require continued analytical and experimental effort. The development of the framework discussed here is intended to permit these efforts to be better focused.

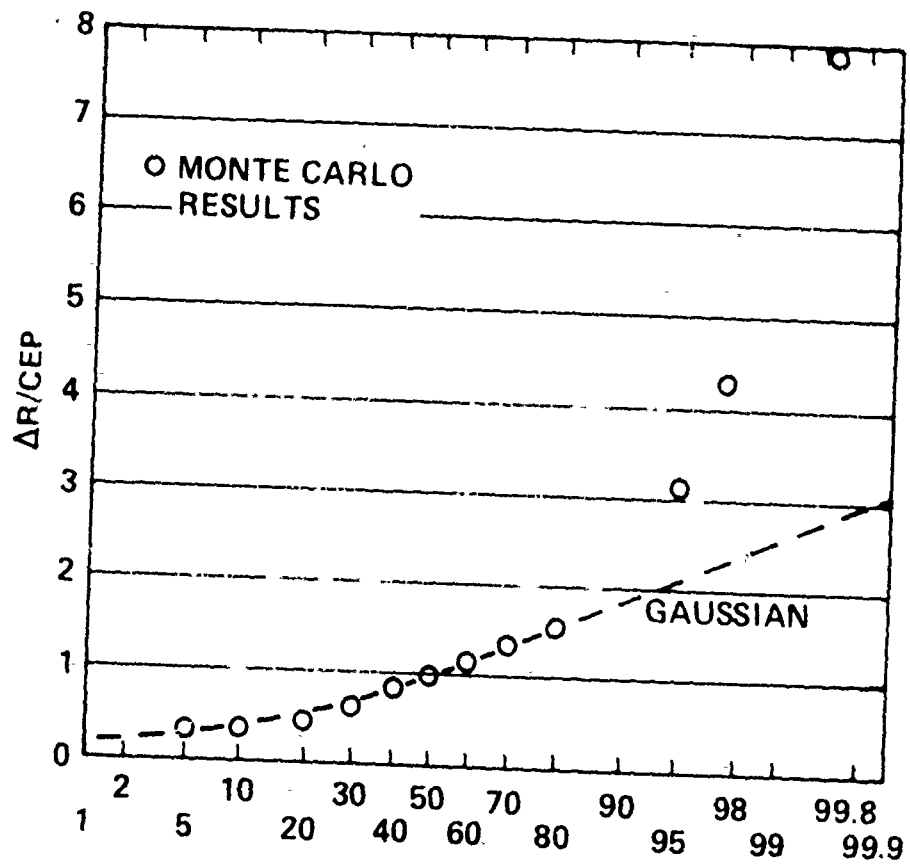


Figure 16. Miss Distance Normalized to CEP Versus Cumulative Probability in Percent

## 8. CONCLUSION

A general computerized framework has been developed for the systematic study of BRV reentry dispersion. It is modular and designed to accommodate improvements in the modeling of dispersion-producing phenomena as they evolve.

## NOMENCLATURE

|   |  |
|---|--|
| A   | base area  |
| $C_{l_0}$   | pure roll torque coefficient   |
| $C_{m_\alpha}, C_{N_\alpha}$  | pitching moment,<br>normal force derivatives   |
| $C_{m_T}, C_{F_T}$  | skewed transition front aerodynamic moment<br>and force coefficients   |
| $\left. \begin{array}{l} \Delta C_{m_{PI}}, \Delta C_{n_{PI}} \\ \Delta C_{Y_{PI}}, \Delta C_{Z_{PI}} \end{array} \right\}$     | skewed transition front incremental plane<br>fixed aerodynamic moment and force<br>coefficients                                    |
| $\Delta C_{m_\delta}, \Delta C_{N_\delta}$  | skewed transition front incremental static<br>moment and force derivatives   |
| $\left. \begin{array}{l} \Delta C_{m_{PII}}, \Delta C_{n_{PII}} \\ \Delta C_{Y_{PII}}, \Delta C_{Z_{PII}} \end{array} \right\}$ | body-fixed incremental aerodynamic forces<br>and moments transformed into plane fixed<br>aerodynamic moment and force coefficients |
| $C_2$   | lateral c. g. offset   |
| d   | reference length   |
| F, G  | discrete roughness transition force and<br>moment functions  |
| h   | tape lap step height   |
| $I_x, I_y, I_z$   | moments of inertia (roll, pitch, yaw)  |
| l   | tape length between tape laps  |
| L   | vehicle length   |
| m   | vehicle mass   |
| p   | roll rate  |

|                        |   |
|------------------------|---|
| $q_{\infty}$           | dynamic pressure  |
| R, S                   | skewed transition front moment and force functions            |
| r                      | radius  |
| $r_n/r_B$              | bluntness ratio - nose to base radius                         |
| $\Delta R_{\max}$      | maximum dispersion in range                                   |
| t                      | time  |
| V                      | relative velocity   |
| $\Delta V$             | induced lateral velocity                                      |
| $X_d/L$                | normalized body-fixed turbulence moment source axial location |
| $\Delta X_d/L$         | $X_d/L$ with respect to transition front                      |
| $\alpha$               | pitch component of angle-of-attack                            |
| $\beta$                | sideslip angle  |
| $\gamma, \Delta\gamma$ | path angle, change in path angle                              |
| $\delta$               | total angle-of-attack   |
| $\theta_c$             | vehicle half cone angle                                       |
| $\lambda$              | tape lap angle  |
| $\nu$                  | heatshield lay-up angle                                       |
| $\rho$                 | atmospheric density   |
| $\sigma$               | transition skew angle   |
| $\phi_d, \Delta\phi_d$ | body-fixed moment meridian location - plane fixed, body fixed |
| $\phi_{TR}$            | transition front tilt angle                                   |
| $\psi$                 | precession angle  |